

Article

Impacts of Stefan Blowing on Hybrid Nanofluid Flow over a Stretching Cylinder with Thermal Radiation and Dufour and Soret Effect

Manoj Kumar Narayanaswamy ¹, Jagan Kandasamy ^{1,*} and Sivasankaran Sivanandam ²

¹ Department of Mathematics, School of Engineering, Presidency University, Bangalore 560064, India

² Department of Mathematics, King Abdulaziz University, Jeddah 21589, Saudi Arabia

* Correspondence: kjaganppmaths@gmail.com

Abstract: The focal interest in this article is to investigate the Stefan blowing and Dufour and Soret effects on hybrid nanofluid (HNF) flow towards a stretching cylinder with thermal radiation. The governing equations are converted into ODE by using suitable transformations. The boundary value problem solver (bvp4c), which is a package in the MATLAB, is used to solve the resulting ODE equations. Results show that rise in the Stefan blowing enhances velocity, temperature, and concentration profiles. Heat transfer rate increases by up to 10% in the presence of 4% nanoparticle/HNF but mass transfer rate diminishes. Additionally, skin friction coefficient, Nusselt number and Sherwood number are examined for many parameters entangled in this article. Additionally, results are deliberately discussed in detail.

Keywords: hybrid nanofluid; Stefan blowing; Dufour and Soret effect; thermal radiation; stretching cylinder



Citation: Narayanaswamy, M.K.; Kandasamy, J.; Sivanandam, S. Impacts of Stefan Blowing on Hybrid Nanofluid Flow over a Stretching Cylinder with Thermal Radiation and Dufour and Soret Effect. *Math. Comput. Appl.* **2022**, *27*, 91. <https://doi.org/10.3390/mca27060091>

Academic Editors: Zhuojia Fu and Gianluigi Rozza

Received: 6 September 2022

Accepted: 31 October 2022

Published: 2 November 2022

Publisher's Note: MDPI stays neutral with regard to jurisdictional claims in published maps and institutional affiliations.



Copyright: © 2022 by the authors. Licensee MDPI, Basel, Switzerland. This article is an open access article distributed under the terms and conditions of the Creative Commons Attribution (CC BY) license (<https://creativecommons.org/licenses/by/4.0/>).

1. Introduction

Recently, many investigators have been drawn in the direction of nano technology because of its significant applications in various industries. Base fluids differ from nanofluids, which have poor heat conductivity in terms of their thermo-physical properties. Choi [1] first introduced nanofluids in 1995 by incorporating nano-sized solid particles into water and claimed that, compared to base fluid, nanofluid has higher thermal conductivity. Such fluids have implications for appliances, which includes refrigerators, processors, cooling systems, hydraulic systems, solar energy machines, biomedical equipment, and microelectronics. Previously, it seems that Crane [2] examined the flow across a linearly stretching surface.

By choosing the proper nanoparticle combination, recent investigators added two different kinds of nanoparticles into the base fluid known as HNF. Specially, nanofluid is well known for having a higher heat transfer rate than regular fluid. Hayat et al. [3] analyzed heat transfer by considering the HNF obtained by the combination of CuO-Ag. Stagnation flow near a stretchy cylinder, along with partial slip condition, was analyzed by Wang [4]. By taking copper and alumina nanoparticles, Maskeen et al. [5] looked into the flow over a stretchy cylinder and the enhancement of heat transfer in HNF. Rehman et al. [6] investigated flow over a stretching sheet with Powell–Eyring fluid model along with joule heating. Salmi et al. [7] examined two-phase chemical reactions HNF flow over a stretchy cylinder. Waini et al. [8] discussed stagnation point HNF flow towards shrinking/stretching cylinder and found that heat transfer rate improved when nanoparticles were present. Waini et al. [9] investigated HNF flow over a shrinking cylinder with prescribed heat flux. Related work is found in Waini et al. [10]. Khashi'ie et al. [11] investigated unsteady squeezing HNF flow over a horizontal channel. Ali et al. [12] analyzed the effect of nonlinear thermal radiation and non-uniform heat flux on hybrid magneto-hydrodynamic (MHD) nanofluid

across a stretching cylinder. Rangi et al. [13] examined the impact of boundary layer flow and variable thermal conductivity towards a stretching cylinder. Natural convection flow over a cylindrical annulus with the effect of either axial or radial magnetic field was examined statistically by Sankar et al. [14]. Siddiqui et al. [15] investigated 3D nanofluid flow over a stretching cylinder with entropy generation. The effect of chemical reactions, thermal radiation, and Carreau fluid flow towards a stretching cylinder was discussed by Lim et al. [16].

Several researchers have studied heat transfer phenomena caused by the concentration and temperature gradients. The mechanism of heat transfer that occurs due to the concentration gradient is called the (diffusion-thermo) Dufour effect, whereas the mechanism of heat transfer that happens due to the temperature gradient is called (thermal-diffusion) Soret effect. These effects are encountered in many practical applications, such as in the areas of geosciences, waste disposal, and chemical engineering, etc. Hayat et al. [17] examined Dufour and Soret effects on the MHD flow of Casson nanofluid and found that temperature field upsurges as the Dufour number rises. Jagan et al. [18] explored at the MHD flow of Jeffrey nanofluid with Dufour and Soret effects in the direction of a stretching cylinder and the results showed that width of the solutal boundary layer increases as the Soret number rises, which lowers the mass transfer rate. Most of the related research was performed by Shaheen et al. [19].

There is no doubt that the thermal radiation effect has been involved in various engineering processes, including die forging, gas turbines, thermal engineering storage and nuclear turbines, etc. Hayat et al. [20] examined Jefferey fluid flow over a stretching cylinder with thermal radiation. The non-linear heat radiation on a 3D unsteady MHD nanofluid flow towards a stretchable surface was examined by Jagan et al. [21]. Gholinia et al. [22] examined the impact of thermal radiation in HNF flow over a porous stretched cylinder. Sreedevi et al. [23] analyzed heat and mass transfer through thermal radiation unsteady HNF flow over a stretching sheet. Waqas et al. [24] investigated thermal transport MHD flow of HNF over a vertical stretching cylinder and found that thermal transport increases as magnetic number rises.

On an impermeable surface, a blowing effect arises. The species (concentration) field and velocity field are related by the Stefan blowing effect, which states that the flow field is directly proportional to the concentration of species. Additionally, some of the applications are found in glass blowing, evaporation in paper drying process, etc. Fang et al. [25] investigated heat and species transfer flow over a stretchy sheet with the effect of Stefan blowing and found that rise in the velocity and concentration profiles as Stefan blowing rises. Rana et al. [26] discovered that reducing the Stefan blowing lowers skin friction while considering non-Fourier and non-Fick's law in their finite element study of bio-convective HNF towards a stretching cylinder. Gowda et al. [27] examined magnetized movement of the Sutterby nanofluid under Stefan blowing conditions and the Cattaneo–Christov concept of heat diffusion.

The current study scrutinized HNF flow with the effect of Stefan blowing, Soret–Dufour, and thermal radiation over a stretchable cylinder, which have yet to be studied. The study of heat and mass transfer in the presence of Stefan blowing and Soret–Dufour effect together is performed in the current work, which shows its novelty. Moreover, the physical quantities of interest are presented for different parameters in the form of tables, 2D graphs, and bar graphs.

2. Mathematical Formulation

Consider an HNF ($\text{Al}_2\text{O}_3\text{-Cu}/\text{H}_2\text{O}$) flow over a stretching cylinder with radius ' a ', as shown in Figure 1. Here, stretching cylinder taken along z -axis and r -axis is perpendicular to it. The free stream velocity and surface velocity are $w_e = 2cz$ and $w_w = 2bz$, where $b > 0$ and $c > 0$ are constants. Stefan blowing, Soret–Dufour and thermal radiation effects are considered.

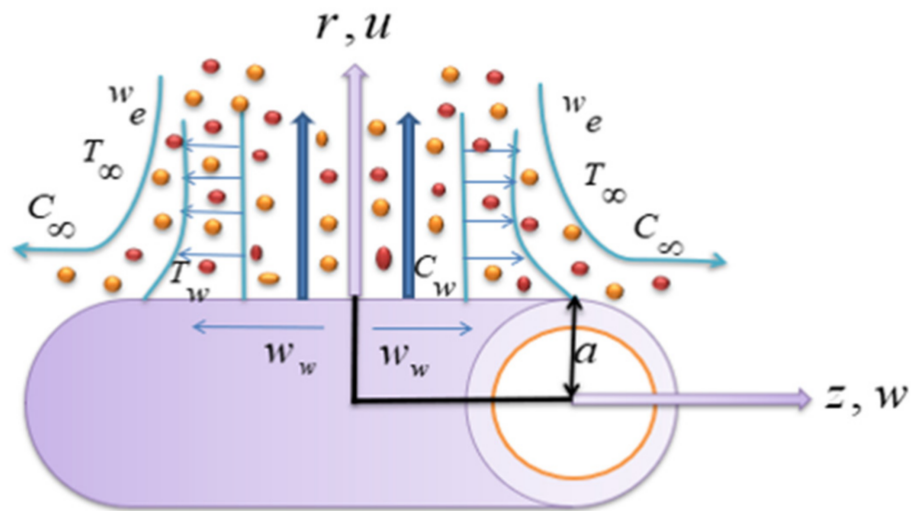


Figure 1. Physical diagram.

The governing equations (referring to Waini et al. [8]) are described as:

Continuity Equation

$$\frac{\partial}{\partial z}(rw) + \frac{\partial}{\partial r}(ru) = 0 \tag{1}$$

Momentum Equation

$$w \frac{\partial w}{\partial z} + u \frac{\partial w}{\partial r} = \frac{\mu_{hmf}}{\rho_{hmf}} \left(\frac{\partial^2 w}{\partial r^2} + \frac{1}{r} \frac{\partial w}{\partial r} \right) + w_e \frac{dw_e}{dz} \tag{2}$$

Temperature Equation

$$\left. \begin{aligned} w \frac{\partial T}{\partial z} + u \frac{\partial T}{\partial r} = \frac{k_{hmf}}{(\rho C_p)_{hmf}} \left(\frac{\partial^2 T}{\partial r^2} + \frac{1}{r} \frac{\partial T}{\partial r} \right) - \frac{1}{(\rho C_p)_{hmf}} \left(\frac{\partial(q_r)}{\partial r} \right) \\ + \frac{Dk_T}{C_s C_p} \left(\frac{\partial^2 C}{\partial r^2} + \frac{1}{r} \frac{\partial C}{\partial r} \right) \end{aligned} \right\} \tag{3}$$

Concentration Equation

$$w \frac{\partial C}{\partial z} + u \frac{\partial C}{\partial r} = D \left(\frac{\partial^2 C}{\partial r^2} + \frac{1}{r} \frac{\partial C}{\partial r} \right) + \frac{Dk_T}{C_s C_p} \left(\frac{\partial^2 T}{\partial r^2} + \frac{1}{r} \frac{\partial T}{\partial r} \right) \tag{4}$$

The associated boundary conditions are:

$$\left. \begin{aligned} u = \frac{-D}{(1-C_w)} \left(\frac{\partial C}{\partial r} \right), w = w_w, T = T_w, C = C_w \text{ at } r = a. \\ w \rightarrow w_e, T \rightarrow T_\infty, C \rightarrow C_\infty \text{ as } r \rightarrow \infty \end{aligned} \right\} \tag{5}$$

where the z - and r - axis' respective velocity components are w and u . T denotes the temperature of HNF. Additionally, the physical features of the HNF are given in Table 1 and the physical attributes of nanoparticles and base fluid are given in Table 2. Here, φ_1 and φ_2 denotes volume fraction of alumina (Al_2O_3) and copper (Cu). The hybrid nanoparticle volume fraction (Al_2O_3 –Cu) φ (referring to Waini et al. [9]) can be written as:

$$\varphi = \varphi_1 + \varphi_2 \tag{6}$$

Table 1. Thermophysical attributes of base fluid (H₂O) and nanoparticles (Al₂O₃ and Cu) (referring to Waini et al. [8]).

Properties	Al ₂ O ₃	Cu	H ₂ O
ρ (kg m ⁻³)	3970	8933	997.1
k (W m ⁻¹ K ⁻¹)	40	400	0.613
C_p (J kg ⁻¹ K ⁻¹)	765	385	4179

Table 2. Thermophysical attributes of nanofluid and HNF (referring to Waini et al. [8]).

Properties	Nanofluid	HNF
Density	$\rho_{nf} = (1 - \varphi_1)\rho_f + \varphi_1\rho_{n1}$	$\rho_{hnf} = (1 - \varphi_2) [(1 - \varphi_1)\rho_f + \varphi_1\rho_{n1}] + \varphi_2\rho_{n2}$
Heat Capacity	$(\rho C_p)_{nf} = (1 - \varphi_1)(\rho C_p)_f + \varphi_1(\rho C_p)_{n1}$	$(\rho C_p)_{hnf} = (1 - \varphi_2) [(1 - \varphi_1)(\rho C_p)_f + \varphi_1(\rho C_p)_{n1}] + \varphi_2(\rho C_p)_{n2}$
Dynamic Viscosity	$\mu_{nf} = \frac{\mu_f}{(1 - \varphi_1)^{2.5}}$	$\mu_{hnf} = \frac{\mu_f}{(1 - \varphi_1)^{2.5}(1 - \varphi_2)^{2.5}}$
Thermal Conductivity	$\frac{k_{nf}}{k_f} = \frac{k_{n1} + 2k_f - 2\varphi_1(k_f - k_{n1})}{k_{n1} + 2k_f + \varphi_1(k_f - k_{n1})}$	$\frac{k_{hnf}}{k_f} = \frac{k_{n2} + 2k_f - 2\varphi_2(k_f - k_{n2})}{k_{n2} + 2k_f + \varphi_2(k_f - k_{n2})}$ where $\frac{k_{nf}}{k_f} = \frac{k_{n1} + 2k_f - 2\varphi_1(k_f - k_{n1})}{k_{n1} + 2k_f + \varphi_1(k_f - k_{n1})}$

The suitable transformations are (referring to Waini et al. [8]):

$$u = -\frac{ca f(\eta)}{\sqrt{\eta}}, w = 2cz f'(\eta), \theta(\eta) = \frac{T - T_\infty}{T_w - T_\infty}, \phi(\eta) = \frac{C - C_\infty}{C_w - C_\infty} \text{ and } \eta = \left(\frac{r}{a}\right)^2. \tag{7}$$

Equation (1) is identically satisfied by Equation (7). By Equation (7), Equations (2)–(5) are reduced as follows:

$$\frac{\mu_r}{\rho_r} [\eta f''' + f''] + \text{Re} [f f'' - f'^2 + 1] = 0, \tag{8}$$

$$\left. \begin{aligned} \frac{k_r}{(\rho C_p)_r} [\eta \theta'' + \theta'] + \frac{2Rd}{3(\rho C_p)_r} [2\eta \theta'' + \theta'] + Du [\eta \phi'' + \phi'] \\ + \text{PrRe} f \theta' = 0 \end{aligned} \right\} \tag{9}$$

$$[\eta \phi'' + \phi'] + Sc Sr [\eta \theta'' + \theta'] + \text{Re} Sc f \phi' = 0, \tag{10}$$

subjected to:

$$\left. \begin{aligned} f(1) = \frac{Sb}{\text{Re} Sc} \phi'(1), f'(1) = \varepsilon, \theta(1) = 1, \phi(1) = 1 \\ f'(\infty) = 1, \theta(\infty) = 0, \phi(\infty) = 0 \end{aligned} \right\}, \tag{11}$$

where $\text{Re} = \frac{ca^2}{2\nu_f}$ represents Reynolds number, $Sb = \frac{(C_w - C_\infty)}{(1 - C_\infty)}$ represents Stefan blowing parameter, $Rd = \frac{4\sigma^* T_\infty^3}{k_f k^*}$ thermal radiation parameter, $Du = \frac{Dk_T(C_w - C_\infty)}{\alpha_f C_s C_p (T_w - T_\infty)}$ Dufour number, $Sc = \frac{\nu_f}{D}$ Schmidt number, $Sr = \frac{Dk_T(T_w - T_\infty)}{\nu_f C_s C_p (C_w - C_\infty)}$ Soret number, $\text{Pr} = \frac{\nu_f}{\alpha_f}$ represents Prandtl number, $\mu_r = \frac{\mu_{hnf}}{\mu_f}$, $\rho_r = \frac{\rho_{hnf}}{\rho_f}$, $k_r = \frac{k_{hnf}}{k_f}$ and $(\rho C_p)_r = \frac{(\rho C_p)_{hnf}}{(\rho C_p)_f}$. Here, the stretching parameter is denoted by $\varepsilon = \frac{b}{c}$.

Equation (12) defines the skin friction coefficient (C_f), Nusselt number (Nu), and Sherwood number (Sh) (referring to Waini et al. [8] and Waqas et al. [24])

$$C_f = \frac{2\tau_w}{\rho_f w_e^2}, Nu = \frac{aq_w}{k_f(T_w - T_\infty)} \text{ and } Sh = \frac{aq_m}{D(C_w - C_\infty)} \tag{12}$$

where shear stress, heat flux, and mass flux are defined as (referring to Waqas et al. [24]):

$$\tau_w = \mu_{hmf} \left(\frac{\partial w}{\partial r} \right)_{r=a}, q_w = -k_{hmf} \left(\frac{\partial T}{\partial r} \right)_{r=a} + q_r \text{ and } q_m = -D \left(\frac{\partial C}{\partial r} \right)_{r=a} \tag{13}$$

Using Equations (7) and (13) in Equation (12), following Equation (14) is obtained.

$$\left(\frac{Re_z}{a} \right) C_f = \frac{\mu_{hmf}}{\mu_f} f''(1), Nu = -2 \left(\frac{k_{hmf}}{k_f} + \frac{4Rd}{3} \right) \theta'(1) \text{ and } Sh = -2\phi'(1). \tag{14}$$

3. Numerical Method

The boundary value problem solver, MATLAB (bvp4c) software, is used to solve Equations (8)–(11) numerically, as described by Waini et al. [8].

Equation (8) is taken as:

$$\left. \begin{aligned} f &= f(1) \\ f' &= f'(1) = f(2) \end{aligned} \right\}' \tag{15a}$$

$$f'' = f'(2) = f(3), \tag{15b}$$

$$f''' = f'(3) = -\frac{1}{\eta} \left\{ \frac{\rho_r}{\mu_r} \text{Re} \left(f(1)f(3) - f(2)^2 + 1 \right) + f(3) \right\}, \tag{15c}$$

Equation (9) becomes:

$$\left. \begin{aligned} \theta &= f(4) \\ \theta' &= f'(4) = f(5) \end{aligned} \right\}' \tag{16a}$$

$$\theta'' = f'(5) = -\frac{1}{\eta} \left\{ \begin{aligned} &1 / \left(k_r + \frac{4Rd}{3} / (\rho C_p)_r - DuScSr \right) \\ &f(5) \left(k_r + \frac{2Rd}{3} / (\rho C_p)_r - ScDuSr + PrRef(1) \right) \\ &+ f(7) Du(ReScf(1) + 1) \end{aligned} \right\}, \tag{16b}$$

Equation (10) becomes:

$$\left. \begin{aligned} \phi &= f(6) \\ \phi' &= f'(6) = f(7) \end{aligned} \right\}' \tag{17a}$$

$$\phi'' = f'(7) = -\frac{1}{\eta} \left\{ \begin{aligned} &f(7) - ScSr \left(1 / \left(k_r + \frac{4Rd}{3} / (\rho C_p)_r - DuScSr \right) \right) \\ &\left[\begin{aligned} &f(5) \left(k_r + \frac{2Rd}{3} / (\rho C_p)_r - ScDuSr + PrRef(1) \right) \\ &+ f(7) Du(ReScf(1) + 1) \end{aligned} \right] \\ &+ ScSr f(5) + ReScf(7) f(1) \end{aligned} \right\}, \tag{17b}$$

with boundary conditions:

$$\left. \begin{aligned} fa(1) &= \frac{Sb}{ReSc} fa(7), fa(2) = \varepsilon, fa(4) = 1, fa(6) = 1 \\ fb(2) &= 1, fb(4) = 0, fb(6) = 0 \end{aligned} \right\}. \tag{18}$$

The necessary solutions are then obtained by solving Equations (15)–(17) using bvp4c MATLAB package.

4. Results and Discussion

In this study, various combinations of important parameters are discussed. The nanoparticle volume fraction of alumina Al_2O_3 (φ_1) and copper Cu (φ_2) changes from 0 to 0.02 (2%). In Table 3, the present results of $f''(1)$ and $-2\theta'(1)$ are in comparison with those of Wang [4] and Waini [8] for different values of Re , and we found that the results display good agreement.

Table 3. Comparison of $f''(1)$ and $-2\theta'(1)$ when $Pr = 6.2$, $\varepsilon = 0$, and $Sb = Sr = Du = Rd = 0$, $\varphi_1 = \varphi_2 = 0$.

Re	$f''(1)$			$-2\theta'(1)$
	Wang [4]	Waini et al. [8]	Present	Present
0.2	0.78604	0.786042	0.786040	1.508638
1	1.48418	1.484183	1.484186	2.793424
10	4.16292	4.162920	4.162921	7.701474

Comparison of C_f and Nu when $\varphi_1 = 0.02$, $Sc = Sb = Sr = Du = Rd = 0$ and $Pr = 6.2$ for different values of ε , φ_2 and Re are given in Table 4. In Table 5, the numerical values of skin friction, Nusselt number, and Sherwood number are presented for different values of Sb , Sr , Du , Rd , ε , and φ_2 .

Table 4. Comparison values of $\left(\frac{Rez}{a}\right)C_f$ and Nu when $Pr = 6.2$, and $Sb = Sr = Du = Rd = 0$.

φ_2	Re	ε	Waini et al. [8]		Present Result	
			$(Rez/a)C_f$	Nu	$(Rez/a)C_f$	Nu
0	0.2	0	0.873892	1.632938	0.873890	1.632940
0.01			-	-	0.946854	1.712795
0.02	0.5	0.2	1.021036	1.792922	1.021036	1.792928
	1		1.457949	2.509315	1.457940	2.509317
	2	0.5	1.092842	4.177081	1.092840	4.177085

Figure 2 depicts the velocity, temperature, and concentration profiles against the Stefan blowing. The boundary layer is growing larger as the blowing parameter rises up to 20%. Physically, the injection of tiny particles (nanoparticles) through the boundary energizes species diffusion as a result the velocity, temperature, and concentration profiles rises.

Increasing the values of φ_2 up to 2% when $\varphi_1 = 0.02$ (2%), $Sb = 0.1$, $\varepsilon = 1.5$, the velocity and temperature profiles decrease slowly (See Figure 3). Physically, an upsurge in the volume fraction can cause the fluid motion to experience resistance, which reduces the fluid motion.

Figure 4a,b show the profile of velocity and temperature decline as the Soret number rises. In fact, an increase in Soret values reduces the viscosity, which provides less resistance and consequently temperature reduces. From Figure 4c, it is shown that concentration profile enhances when elevating the Soret number. This figure gives the impression that as the Soret number rises, the fluid concentration profile rises as a result of temperature gradients influencing species diffusion. From Figure 5a, it is shown that increasing the Dufour number causes decline in the temperature field. As a result, the fluid receives less heat and its viscosity increases. In Figure 5b, the concentration profile slightly increases due to low friction, which, in turn, enhances the concentration. The thickness of thermal boundary layer decreases as thermal radiation increase. This is because large values of

radiation parameter correspond to an increase in dominance of conduction over radiation, thereby decreasing the thickness of thermal boundary layer and increasing the heat loss at the ambient temperature (see Figure 6a). Meanwhile, a similar trend is observed in the concentration boundary layer thickness, with higher values of radiation parameters (see Figure 6b).

In Figure 7a, while increasing the value of φ_1 and φ_2 (up to 2%), the skin friction coefficient is found to be decreasing. At $\varepsilon = 1$, the C_f is found to be zero because the surface velocity is equal to free stream velocity. For $\varepsilon < 1$, C_f is positive because the surface velocity is greater than the free stream velocity and vice versa is found in case of $\varepsilon > 1$. From Figure 7b, the Nusselt number is increasing while the value of φ_1 and φ_2 is increasing (up to 2%). Figure 7c, the Sherwood number increases slightly alongside the increase in the nanoparticle volume fraction of φ_1 and φ_2 (up to 2%).

Figure 8a,b display the different values of Sb when $Sc = 0.6$, $Sr = Rd = Du = 0.2$, $Pr = 6.2$, and $\varphi_1 = \varphi_2 = 0.02$. The Nusselt number decreases as the blowing parameter increases, which results in a decrease in the heat transfer rate. Additionally, this plot shows that the effect of Sb is less dominant, in comparison to thermal radiation. The Sherwood number increases with increasing of Sb . Physically, an increase in mass blowing at surface results in an increase in the mass flow rate.

Figure 9a displays the different values of Rd when $Sc = 0.6$, $Sr = Du = 0.2$, $Pr = 6.2$, and $\varphi_1 = \varphi_2 = 0.02$. Nu increases with rising thermal radiation parameter because there will be a rise in temperature within the boundary layer. Additionally, Figure 9b shows that the heat transfer rate increases with an increase in Dufour number. Physically, Du relates to the effect of concentration gradient to the thermal energy flux in the flow.

Table 5. Numerical values of $(Re_z/a)C_f$, Nu and Sh when $Pr = 6.2$, $Re = 1$ and $\varphi_1 = 0.02$.

Sb	Sr	Du	Rd	"	' ₂	$(Re_z/a)C_f$	Nu	Sh
0.0	0.1	0.1	0.1	0.3	0.02	1.312229	5.235561	2.147327
0.1	-	-	-	-	-	1.356625	3.852460	2.181614
1.0	-	-	-	-	-	0.899479	0.015974	1.434119
2.0	-	-	-	-	-	0.699197	0.000416	1.031123
-	0.2	-	-	-	-	0.687271	0.000026	1.061832
-	0.3	-	-	-	-	0.676204	-0.000335	1.090929
-	0.4	-	-	-	-	0.637198	-0.000383	1.123820
-	-	0.2	-	-	-	0.658677	-0.001201	1.120188
-	-	0.3	-	-	-	0.658589	-0.001785	1.20365
-	-	0.4	-	-	-	0.658499	-0.002355	1.120542
-	-	-	0.2	-	-	2.083692	21.114771	0.253986
-	-	-	0.4	-	-	1.810421	20.757020	0.505700
-	-	-	0.6	-	-	1.690819	22.816878	0.465192
-	-	-	-	0.1	-	2.124273	22.499878	0.458991
-	-	-	-	0.2	-	0.711615	-0.003096	1.103116
-	-	-	-	0.3	-	1.690819	22.816878	0.465192
-	-	-	-	-	0.01	0.657825	-0.004825	1.122316
-	-	-	-	-	0.015	0.657825	-0.004825	1.122316
-	-	-	-	-	0.02	0.657825	-0.004825	1.122316

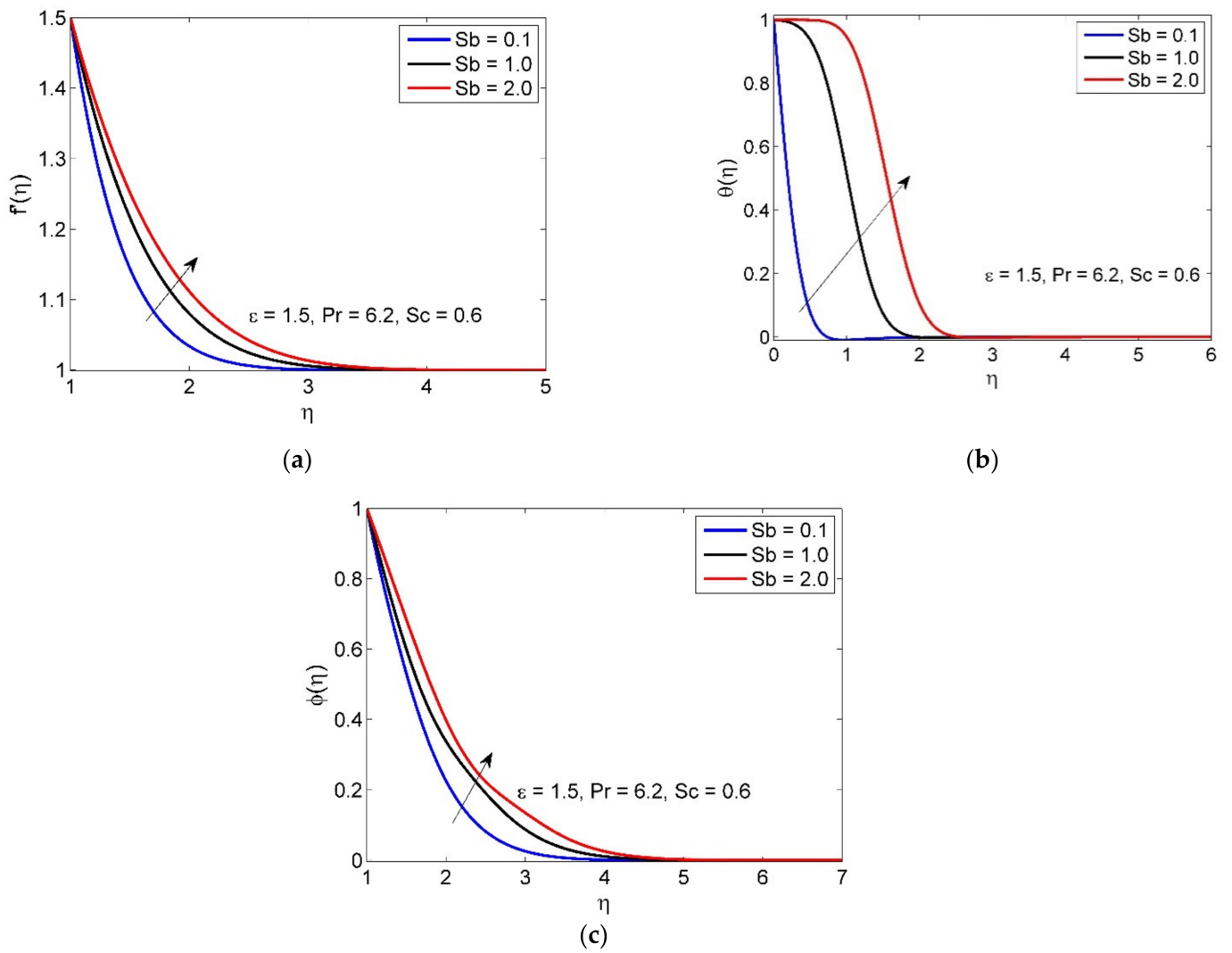


Figure 2. Influences of S_b on $f'(\eta)$, $\theta(\eta)$ and $\phi(\eta)$.

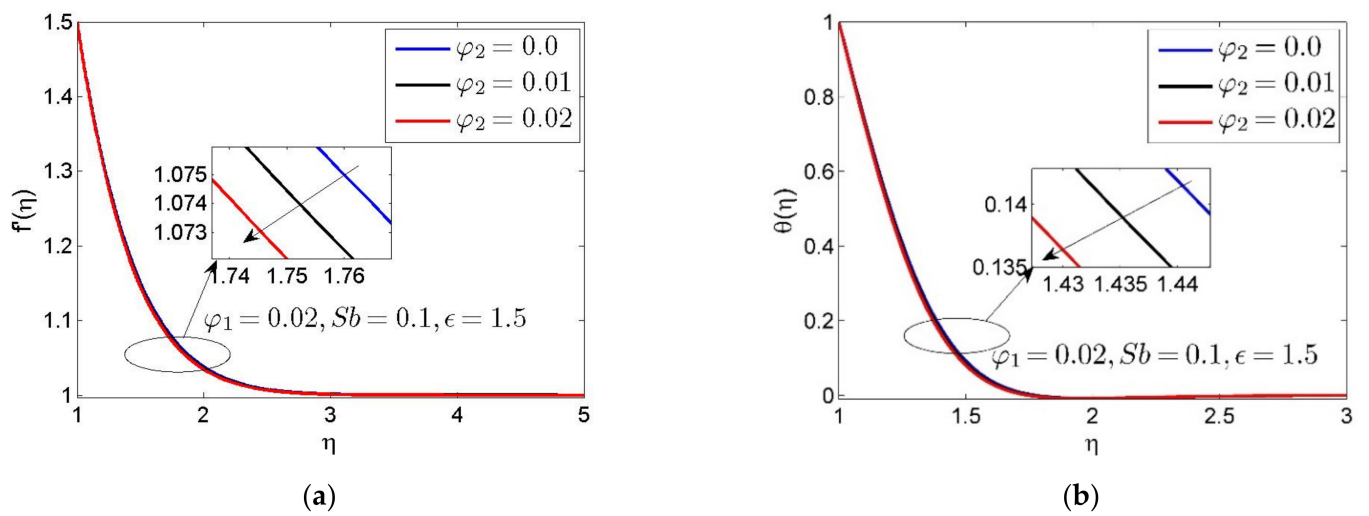


Figure 3. Influences of φ_2 on $f(\eta)$ and $\theta(\eta)$.

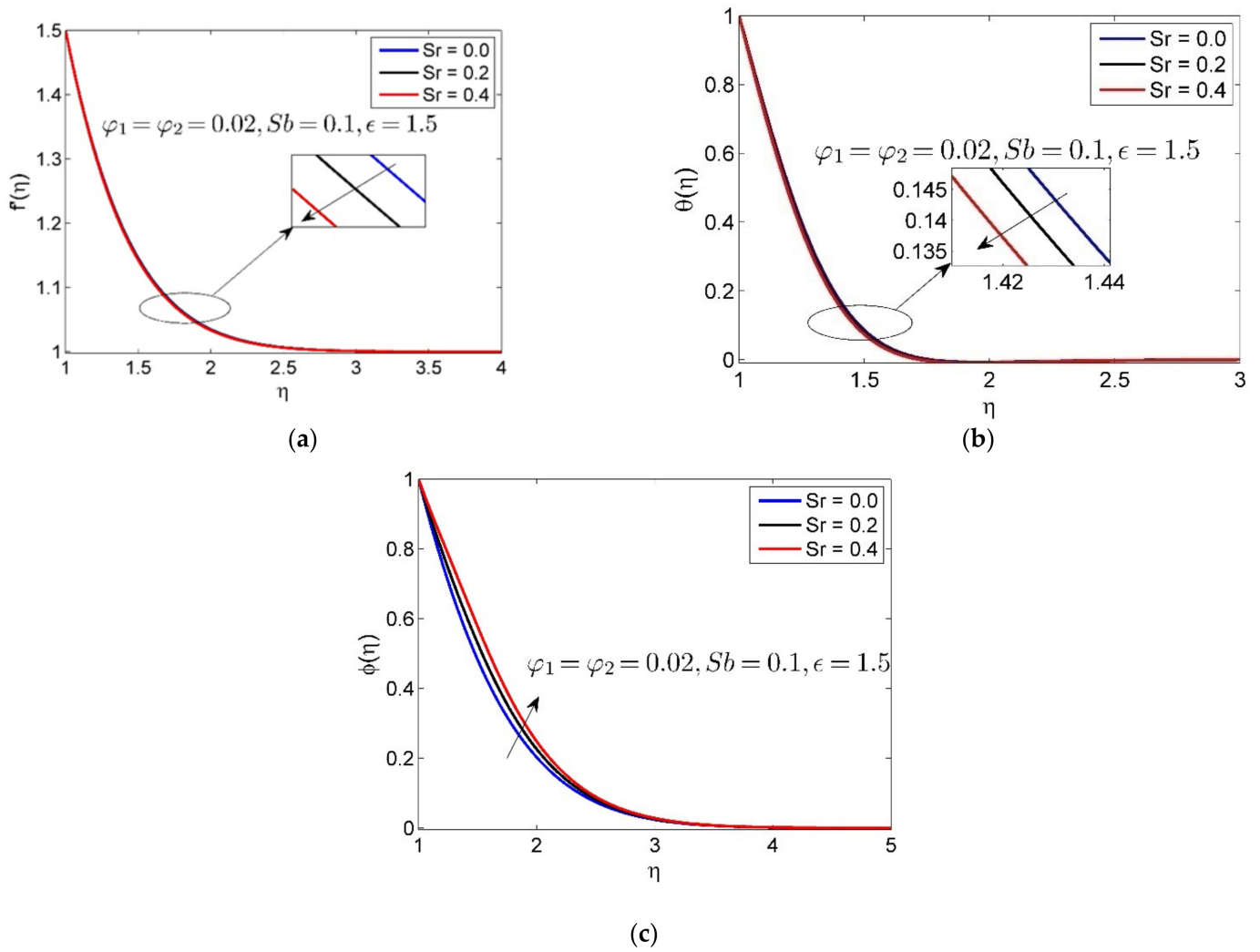


Figure 4. Influences of Sr on $f(\eta)$ and $\theta(\eta)$ and $\phi(\eta)$.

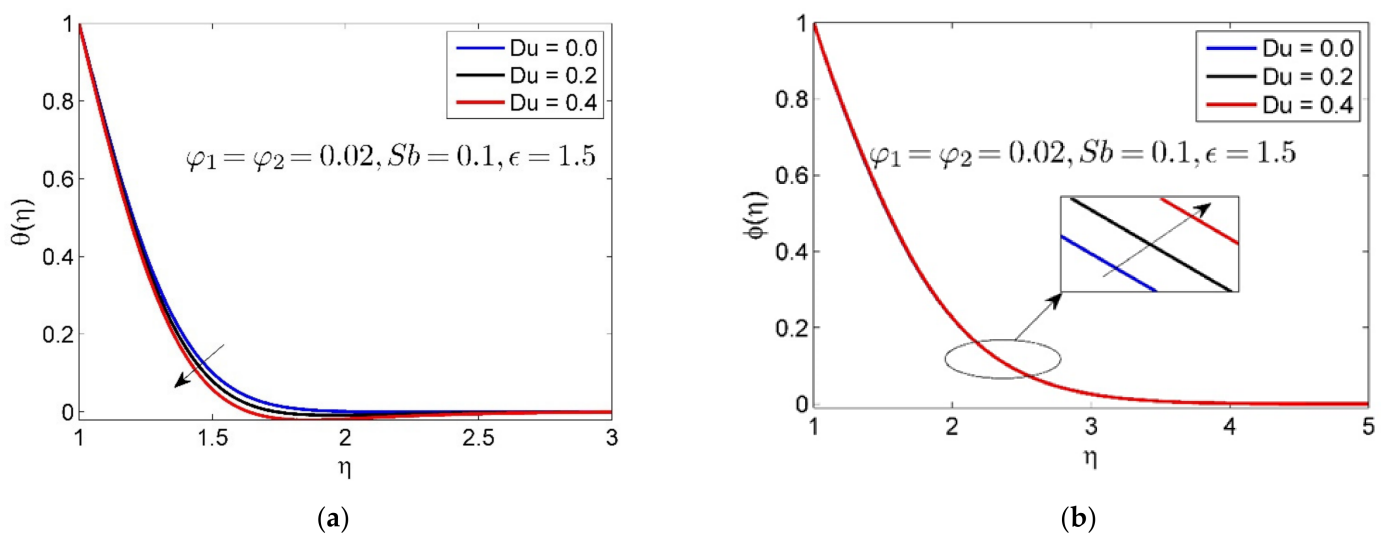


Figure 5. Influences of Du on $\theta(\eta)$ and $\phi(\eta)$.

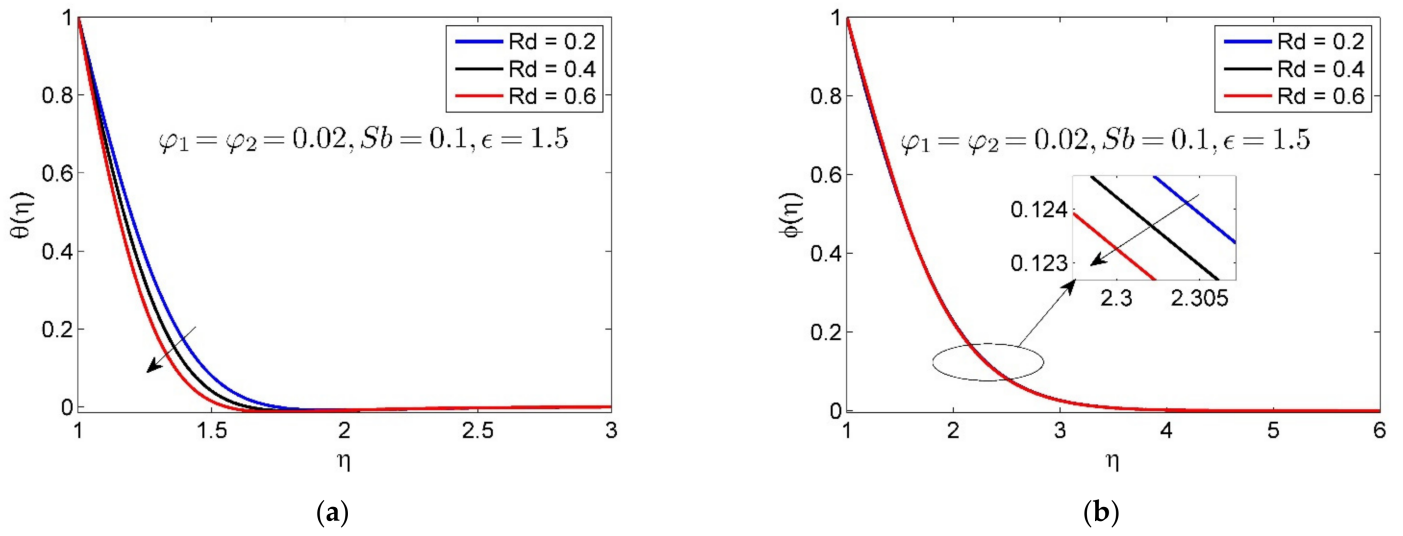


Figure 6. Influences of Rd on $\theta(\eta)$ and $\phi(\eta)$.

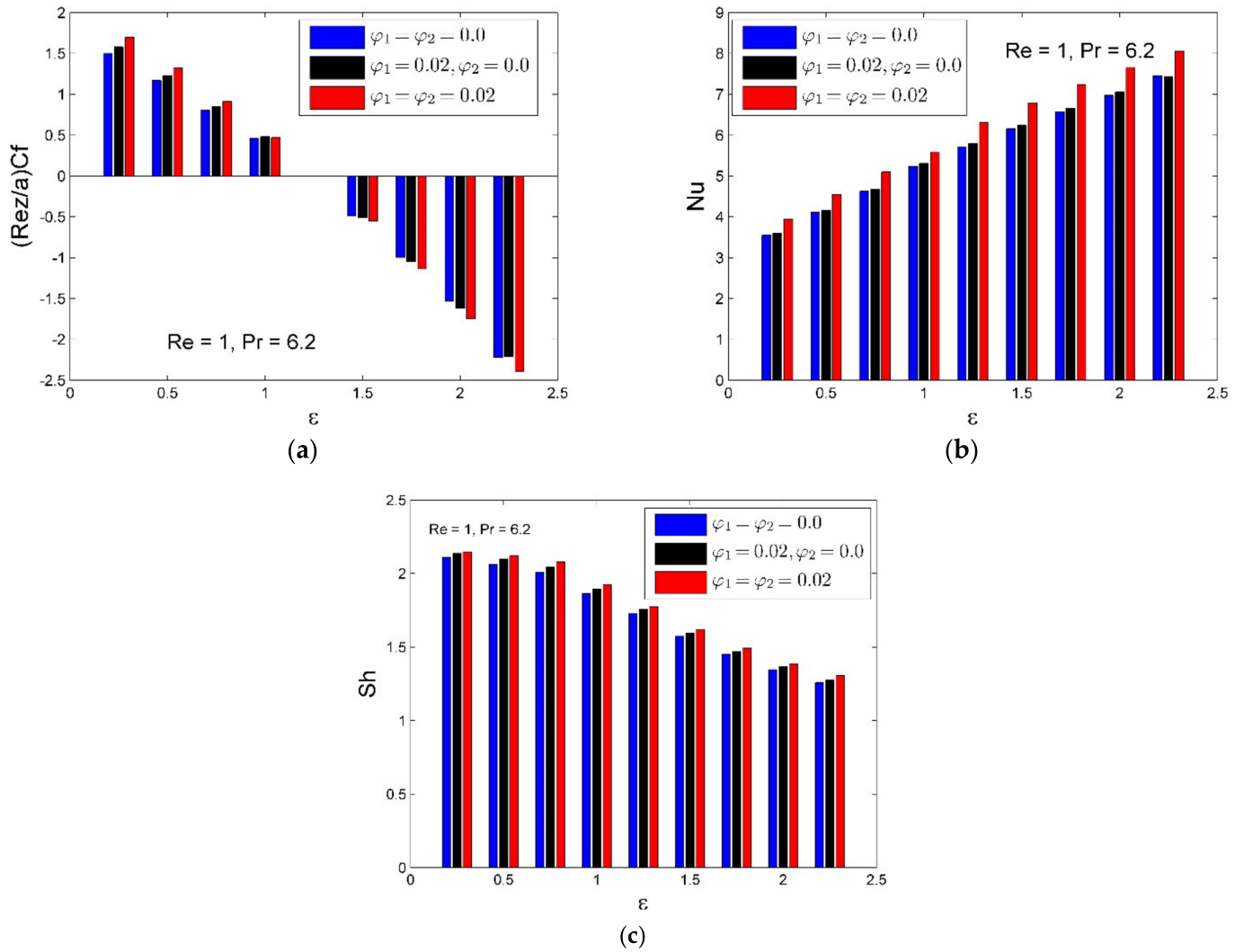


Figure 7. Influences of φ_1 and φ_2 on C_f , Nu , and Sh .

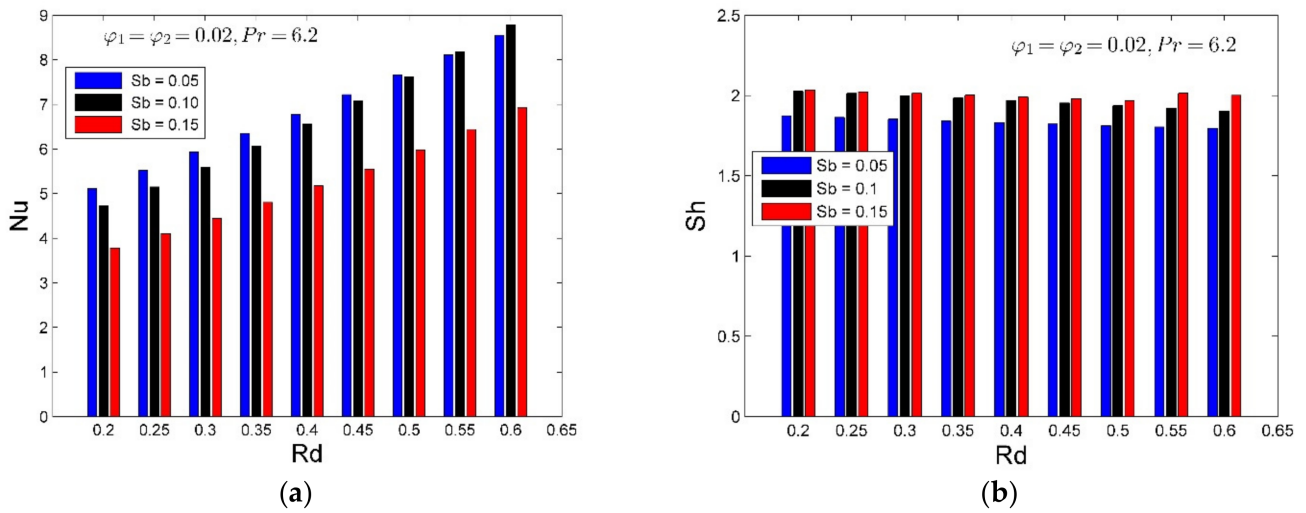


Figure 8. Influences of S_b on Nu and Sh .

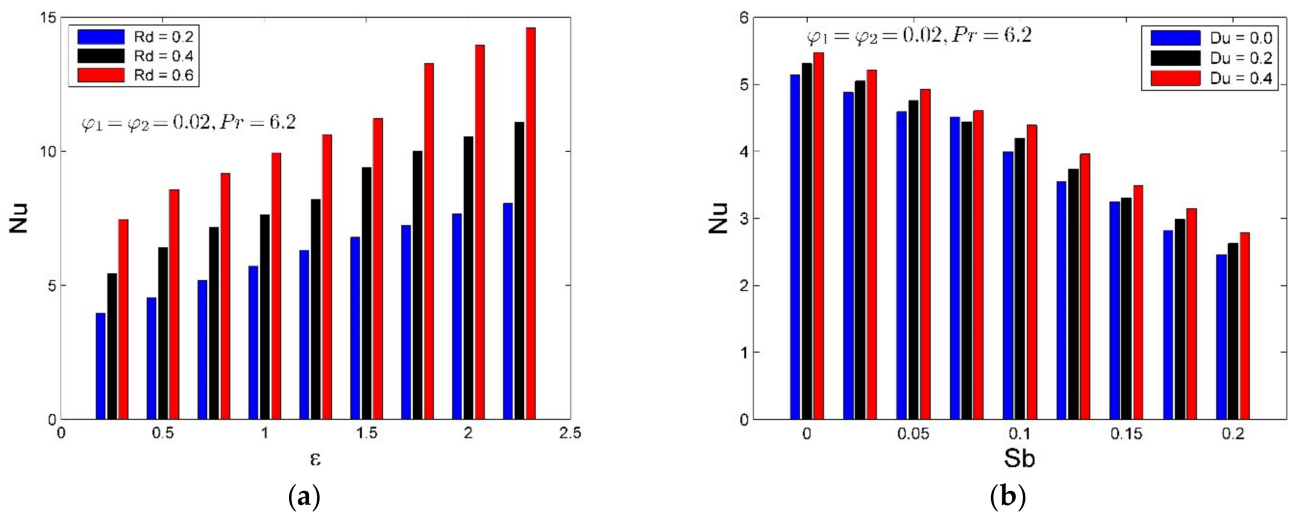


Figure 9. Influences of Rd and Du on Nu .

Increasing the Soret number decreases the mass transfer rate. Further, the Soret effect is the cause of the diffusion of species from higher to lower concentration due to temperature gradient and, as a result, mass transfer rate diminishes, as shown in Figure 10.

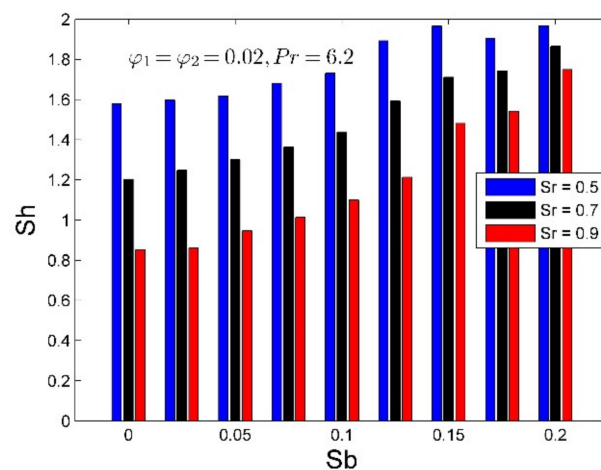


Figure 10. Influences of S_r on Sh .

5. Conclusions

In this study, the impact of Stefan blowing, Soret, Dufour and thermal radiation on HNF flow towards a stretching cylinder has been accomplished.

This study has the following potential limitations:

- The Schmidt number is fixed in our model as water is taken as the base fluid.
- The Stefan blowing effect only arises at the impermeable surface and perpendicular to the flow direction.
- The value of the Prandtl number is dependent on the base fluid, so it ranges from 1.7 to 13.7.
- The main fallout of the current study is listed below as follows:
- As Stefan blowing intensifies, the thickness of the velocity, thermal, and concentration boundary layers grows. As a result, the heat transfer rate declines while the mass transfer rate rises.
- The convective heat transfer and mass transfer rate is improved by up to 20% with the inclusion of HNF 2%.
- Concentration (temperature) boundary layer enhanced (declines) by evaluating the Dufour and Soret numbers.
- The inclusion of thermal radiation improved the heat transfer rate as the stretching parameter increases.
- Higher values of Soret number reduce the mass transfer rate, while Stefan blowing parameter has a contrary impact on it.

Author Contributions: Conceptualization, J.K. and S.S.; methodology, J.K.; software, J.K. and M.K.N.; validation, J.K.; formal analysis, J.K, S.S. and M.K.N.; investigation, J.K.; resources, J.K.; writing—original draft preparation, J.K. and M.K.N.; writing—review and editing, J.K.; visualization, J.K.; supervision, J.K. All authors have read and agreed to the published version of the manuscript.

Funding: This research received no external funding.

Conflicts of Interest: The authors declare no conflict of interest.

Abbreviations

In this manuscript, the following abbreviations are used.

HNF Hybrid nanofluid
MHD Magnetohydrodynamics

Nomenclature

w, u	velocity components taken along z - and r -axis ($\text{m}\cdot\text{s}^{-1}$)
w_w	surface velocity
T_w	surface temperature
C_w	surface concentration
w_e	free stream velocity
T_∞	ambient temperature
C_∞	ambient concentration
a	cylinder radius (m)
Du	Dufour number
Sr	Soret number
D	mass diffusivity ($\text{m}^2\cdot\text{s}^{-1}$)
k^*	mean absorption coefficient ($\text{c}\cdot\text{m}^{-1}$)
q_r	heat flux ($\text{kg}\cdot\text{m}^2\cdot\text{s}^{-3}$)
k_T	thermal diffusion ratio
C_s	concentration susceptibility
C_p	specific heat ($\text{kg}^{-1}\cdot\text{J}$)
T	temperature of the fluid (K)

C	concentration of the fluid
k	thermal conductivity
Pr	Prandtl number
Rd	thermal radiation parameter
Sc	Schmidt number
Re	local Reynolds number
C_f	skin friction coefficient
Nu	Nusselt number
Sh	Sherwood number
Sb	Stefan blowing parameter

Greek Symbols

ν	kinematic viscosity of the fluid ($\text{m}^2 \cdot \text{s}^{-1}$)
ρ	density of the fluid ($\text{kg} \cdot \text{m}^{-3}$)
σ^*	Stefan-Boltzmann constant ($\text{W} \cdot \text{m}^{-2} \cdot \text{K}^{-4}$)
μ	dynamic viscosity of the fluid ($\text{m}^2 \cdot \text{s}^{-1}$)
α	thermal diffusivity ($\text{m}^2 \cdot \text{s}^{-1}$)
ε	stretching parameter

Subscripts

∞	ambient
f	base fluid
nf	nanofluid
hnf	hybrid nanofluid

References

- Choi, S.U.; Eastman, J.A. *Enhancing Thermal Conductivity of Fluids with Nanoparticles*; Argonne National Lab (ANL): Argonne, IL, USA, 1995.
- Crane, L.J. Flow past a stretching plate. *Z. Angew. Phys. ZAMP* **1970**, *21*, 645–647. [[CrossRef](#)]
- Hayat, T.; Nadeem, S. Heat transfer enhancement with Ag–CuO/water hybrid nanofluid. *Results Phys.* **2017**, *7*, 2317–2324. [[CrossRef](#)]
- Wang, C.Y. Stagnation flow on a cylinder with partial slip—An exact solution of the Navier–Stokes equations. *IMA J. Appl. Math.* **2007**, *72*, 271–277. [[CrossRef](#)]
- Maskeen, M.M.; Zeeshan, A.; Mehmood, O.U.; Hassan, M. Heat transfer enhancement in hydromagnetic alumina–copper/water hybrid nanofluid flow over a stretching cylinder. *J. Therm. Anal. Calorim.* **2019**, *138*, 1127–1136. [[CrossRef](#)]
- Rehman, S.; Anjum, A.; Farooq, M.; Hashim; Malik, M.Y. Melting heat phenomenon in thermally stratified fluid reservoirs (Powell–Eyring fluid) with joule heating. *Int. Commun. Heat Mass Transf.* **2022**, *137*, 106196. [[CrossRef](#)]
- Salmi, A.; Madkhali, H.A.; Nawaz, M.; Alharbi, S.O.; Malik, M.Y. Non-Fourier modeling and numerical simulations on heat and transfer in tangent hyperbolic nanofluid subjected to chemical reactions. *Int. Commun. Heat Mass Transf.* **2022**, *134*, 105996. [[CrossRef](#)]
- Waini, I.; Ishak, A.; Pop, I. Hybrid nanofluid flow towards a stagnation point on a stretching/shrinking cylinder. *Sci. Rep.* **2020**, *10*, 9296. [[CrossRef](#)]
- Waini, I.; Ishak, A.; Pop, I. Hybrid Nanofluid Flow on a Shrinking Cylinder with Prescribed Surface Heat Flux. *Int. Numer. Methods Heat Fluid Flow* **2020**, *31*, 1987–2004. [[CrossRef](#)]
- Waini, I.; Ishak, A.; Pop, I. Hybrid Nanofluid Flow over a Permeable Non-Isothermal Shrinking Surface. *Mathematics* **2021**, *9*, 538. [[CrossRef](#)]
- Khashi'ie, N.S.; Waini, I.; Arifin, N.M.; Pop, I. Unsteady Squeezing Flow of Cu–Al₂O₃/Water Hybrid Nanofluid in a Horizontal Channel with Magnetic Field. *Sci. Rep.* **2021**, *11*, 14128. [[CrossRef](#)]
- Ali, A.; Kanwal, T.; Awais, M.; Shah, Z.; Kumam, P.; Thounthong, P. Impact of thermal radiation and non-uniform heat flux on MHD hybrid nanofluid along a stretching cylinder. *Sci. Rep.* **2021**, *11*, 20262. [[CrossRef](#)]
- Rangi, R.R.; Ahmad, N. Boundary layer flow past a stretching cylinder and heat transfer with variable thermal conductivity. *Appl. Math.* **2012**, *3*, 205–209. [[CrossRef](#)]
- Sankar, M.; Venkatachalappa, M.; Shivakumara, I.S. Effect of magnetic field on natural convection in a vertical cylindrical annulus. *Int. J. Eng. Sci.* **2006**, *44*, 1556–1570. [[CrossRef](#)]
- Siddiqui, B.K.; Batool, S.; Mahmood ul Hassan, Q.; Malik, M.Y. Repercussions of Homogeneous and Heterogeneous Reactions of 3D Flow of Cu-Water and Al₂O₃-Water Nanofluid and Entropy Generation Estimation along Stretching Cylinder. *Ain Shams Eng. J.* **2022**, *13*, 101493. [[CrossRef](#)]
- Lim, Y.J.; Shafie, S.; Isa, S.M.; Rawi, N.A.; Mohamad, A.Q. Impact of chemical reaction, thermal radiation and porosity on free convection Carreau fluid flow towards a stretching cylinder. *Alex. Eng. J.* **2022**, *61*, 4701–4717. [[CrossRef](#)]

17. Hayat, T.; Shehzad, S.A.; Alsaedi, A. Soret and Dufour effects on magnetohydrodynamic (MHD) flow of Casson fluid. *Appl. Math. Mech.* **2012**, *33*, 1301–1312. [[CrossRef](#)]
18. Jagan, K.; Sivasankaran, S.; Bhuvaneswari, M.; Rajan, S.; Makinde, O.D. Soret and Dufour effect on MHD Jeffrey nanofluid flow towards a stretching cylinder with triple stratification, radiation and slip. *Defect Diffus. Forum* **2018**, *387*, 523–533. [[CrossRef](#)]
19. Shaheen, N.; Alshehri, H.M.; Ramzan, M.; Shah, Z.; Kumam, P. Soret and Dufour effects on a Casson nanofluid flow past a deformable cylinder with variable characteristics and Arrhenius activation energy. *Sci. Rep.* **2021**, *11*, 19282. [[CrossRef](#)]
20. Hayat, T.; Asad, S.; Alsaedi, A.; Alsaadi, F.E. Radiative Flow of Jeffrey Fluid through a Convectively Heated Stretching Cylinder. *J. Mech.* **2014**, *31*, 69–78. [[CrossRef](#)]
21. Jagan, K.; Sivasankaran, S.; Bhuvaneswari, M.; Rajan, S. Effect of non-linear radiation on 3D unsteady MHD nanoliquid flow over a stretching surface with double stratification. In *Applied Mathematics and Scientific Computing*; Birkhäuser: Cham, Switzerland, 2019; pp. 109–116.
22. Gholinia, M.; Armin, M.; Ranjbar, A.A.; Ganji, D.D. Numerical Thermal Study on CNTs/C₂H₆O₂-H₂O Hybrid Base Nanofluid upon a Porous Stretching Cylinder under Impact of Magnetic Source. *Case Stud. Therm. Eng.* **2019**, *14*, 100490. [[CrossRef](#)]
23. Sreedevi, P.; Sudarsana Reddy, P.; Chamkha, A. Heat and Mass Transfer Analysis of Unsteady Hybrid Nanofluid Flow over a Stretching Sheet with Thermal Radiation. *SN Appl. Sci.* **2020**, *2*, 1222. [[CrossRef](#)]
24. Waqas, H.; Raza Shah Naqvi, S.M.; Alqarni, M.S.; Muhammad, T. Thermal Transport in Magnetized Flow of Hybrid Nanofluids over a Vertical Stretching Cylinder. *Case Stud. Therm. Eng.* **2021**, *27*, 101219. [[CrossRef](#)]
25. Fang, T.; Jing, W. Flow, heat, and species transfer over a stretching plate considering coupled Stefan blowing effects from species transfer. *Commun. Nonlinear Sci. Numer. Simul.* **2014**, *19*, 3086–3097. [[CrossRef](#)]
26. Rana, P.; Makkar, V.; Gupta, G. Finite element study of bio-convective Stefan blowing Ag-MgO/water hybrid nanofluid induced by stretching cylinder utilizing non-Fourier and non-Fick's laws. *Nanomaterials* **2021**, *11*, 1735. [[CrossRef](#)]
27. Gowda, R.J.; Kumar, R.N.; Rauf, A.; Prasannakumara, B.C.; Shehzad, S.A. Magnetized flow of Sutterby nanofluid through Cattaneo-Christov theory of heat diffusion and Stefan blowing condition. *Appl. Nanosci.* **2021**. [[CrossRef](#)]